Full-Wave Lens Antenna Analysis With the Proxy Sources Method

Ozzola, Riccardo; Tadolini, Cesare; Speksnijder, Erik A.; Neto, Andrea

DOI
10.1109/TAP.2025.3567458

Publication date
2025

Document Version
Final published version

Published in
IEEE Transactions on Antennas and Propagation

Communication

Full-Wave Lens Antenna Analysis With the Proxy Sources Method

Riccardo Ozzola, Cesare Tadolini, Erik A. Speksnijder, and Andrea Neto

***Abstract*—This communication presents a method to ease the computational burden of simulating antennas radiating close to dielectric bodies, e.g., dielectric lenses. The input impedance can be split into the capacitance of the feeding gap, a term associated with the propagation in dielectric half-space, and a term associated with the reflections created by the finite dielectric. These three terms are independent of each other and can be calculated separately. The capacitance of the feed and the term associated with radiation in the absence of the reflections can be easily evaluated. A feed with coarser detail and having the same interaction with the lens is then synthesized. This allows us to estimate the reflection from the lens efficiently, and then the different terms are recombined to estimate the total input impedance.**

***Index Terms*—Equivalent circuit, lens antennas, method of moments.**

I. Introduction

In the sub-mm wave domain, some of the most successful examples of front-end integration resort to lens antennas [1], [2], [3], [4], [5], [6], [7], [8]. The analysis and design of such antennas typically require the accurate modeling of the input impedance, mutual coupling, and radiation patterns. Due to the electrically large size of the lenses, high-frequency techniques, such as the physical optics (PO) [1], have played a major role in easing the analysis of quasi-optical systems, allowing to avoid time-consuming full-wave simulations.

Recently, small-size lens antennas have gained popularity due to their flexibility. These have been used as the elements for coherent arrays [9] or as the core in the core-shell lens architecture [10]. In these cases, the PO based on ray tracing [1], [11], [12], [13], [14], [15], [16], [17], [18], [19], [20], [21] becomes inaccurate [22] because the curvature of the surfaces is small with respect to the wavelength. These limitations call for developing analysis techniques that allow for efficient simulations without compromising the accuracy.

For these reasons, full-wave solvers must be used to analyze dielectric lenses, including also their integrated feed [Fig. 1(a)]. However, in the sub-mm wave regime, the thickness of the metal cannot be neglected, as it is comparable with the other design parameters and impacts performance [23], [24]. The modeling of the feed with its metal thickness yields challenging multiscale simulations, which might have long simulation times.

To circumvent this issue, a strategy to decouple the analysis of the feed from the lens is developed. The lens creates the reflections coming from its boundaries, which are wave phenomena generated at a distance from the feed, and therefore, weakly dependent on its specific geometry. A proxy dipole is synthesized with a much coarser discretization such that it radiates equivalently into the dielectric half-space having the same permittivity of the lens Fig. 1(b). This allows to study the proxy problem Fig. 1(c) with a much coarser mesh and improved solution times.

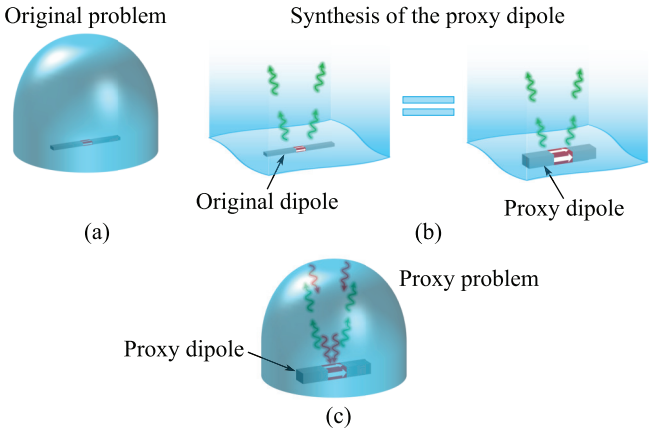

Fig. 1. Representation of (a) original problem, (b) synthesis of the proxy dipole in the absence of the reflections, and (c) proxy problem.

This approach is independent of the specific numerical technique used. It finds its largest benefit when structured meshes are used, but it can also be applied for unstructured meshes when a large imbalance between the feed size and its surroundings is present.

II. Equivalent Circuit of a Dipole Illuminating a Dielectric Lens

A. Dynamic and Quasi-Static Component

From the derivation in [23], the input impedance Z_{in} of a dipole can be approximated, as shown in Fig. 2(a), as the parallel between the quasi-static component Z_{qs}, associated with the capacitance of the gap and the dynamic impedance Z_{dyn}, associated with a wave propagating on the dipole and causing the radiation. In the spectral domain, Z_{dyn} corresponds to the low part of the spectrum, which is dominated by a pole, while Z_{qs} is associated with the high part of the plane-wave spectrum.

B. Reflection Component of the Input Impedance

The input impedance of any antenna is defined as the ratio between integrals on the input ports of the electric field and the magnetic field when one of the two fields is assumed to be the excitation and the other is the unknown of the problem. If a dielectric body is present, a fraction of the radiated fields is reflected by the dielectric-air interface back to the feeding ports, changing the impedance (or the admittance) with respect to the case without the reflections [25]. As the reflections are due to radiative phenomena, these are associated with the dynamic component of the impedance (or the

Received 13 December 2024; revised 28 April 2025; accepted 29 April 2025. Date of publication 12 May 2025; date of current version 6 August 2025. *(Corresponding author: Riccardo Ozzola.)*

The authors are with the Microelectronics Department, Electrical Engineering, Mathematics and Computer Science Faculty, Delft University of Technology, 2628 Delft, The Netherlands (e-mail: R.Ozzola-1@tudelft.nl).

This article has supplementary downloadable material available at https://doi.org/10.1109/TAP.2025.3567458, provided by the authors.

Digital Object Identifier 10.1109/TAP.2025.3567458

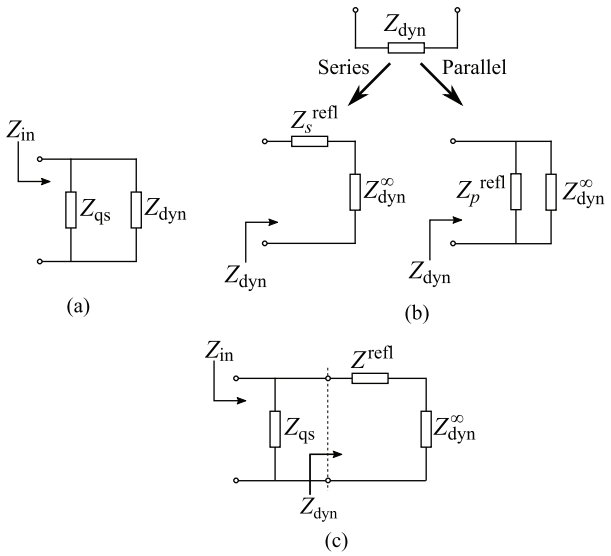

Fig. 2. Equivalent circuit representation of (a) parallel of the dynamic and the quasi-static components of the input impedance, (b) dynamic component of the input impedance with the series and parallel representation of the reflections, and (c) complete equivalent circuit of an integrated lens antenna.

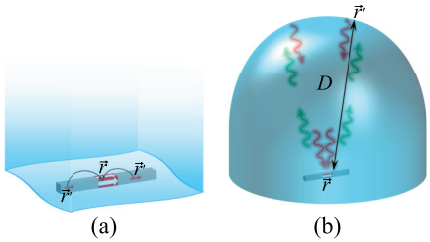

Fig. 3. Representation of (a) near-field interaction in the feed and (b) direct radiation and the reflections from the lens.

admittance). As the antenna input port can be arbitrarily represented with a series or parallel equivalent circuit [Fig. 2(b)], the correction due to the reflections can be added to the dynamic component calculated in the absence of the reflections. Consequently, the dynamic component of the input impedance or admittance can be expressed as follows:

$$Z_{\text{dyn}} = Z_{\text{dyn}}^{\infty} + Z_s^{\text{refl}} \tag{1}$$

$$Y_{\text{dyn}} = Y_{\text{dyn}}^{\infty} + Y_p^{\text{refl}} \tag{2}$$

where Z_{dyn}^{∞} and Y_{dyn}^{∞} are the dynamic components of the impedance and the admittance, respectively, calculated without the reflections, and Z_s^{refl} and Y_p^{refl} are the impedance and admittance, respectively, associated with the reflections. The values of the impedance added in series or parallel are generally different. As in the following, we intend to work with the impedance, we always refer to the series model (1), and to avoid redundancy, the subscript s is, from now on, omitted.

It is important to stress how Z_{dyn}^{∞} and Z_s^{refl} depend on the near-field and the far-field of the feed. The fields required for the evaluation of the impedances of (1) are observed in the gap at $\vec{r}$ and are generated by the equivalent currents at $\vec{r}'$, induced by the excitation. The field in the absence of the reflections, i.e., the one associated with Z^{∞}, is evaluated in the near-field of the dipole, and it has a fast space variability being calculated with Green's function $\propto |\vec{r} - \vec{r}'|^{-3}$ [Fig. 3(a)]. On the contrary, if the boundaries of the dielectric are sufficiently distant from the dipole, to be outside from the reactive region of the dipole, the field associated with the reflections varies less rapidly as the field propagates from the dipole to the boundaries and backward, with a path length D, having a length of the same order of the diameter [Fig. 3(b)], and Green's function of the reflections is dominated by the term $\propto (|\vec{r} - \vec{r}'| + D)^{-1}$. Due to its fast space variability, the impedance calculated without the reflections depends on the specific geometry, while the impedance associated with the reflections depends mainly on the dynamic component of the currents and not on the specific shape of the feed.

The proxy sources method can be extended to the analysis of lens arrays. As these are sparsely sampled, all the reactive zones of the feeds include only the pertinent element. The outward contribution can still be split from the reflected term. However, the proxy feeds must be synthesized to account for the array environment.

III. Input Impedance Calculation With the Proxy Sources Method

The proxy dipole is characterized by a discretization coarser than the original one, but it radiates equivalently in the absence of the reflections, as shown in Fig. 1(b). This constraint is expressed by the following condition:

$$\text{Re}\left\{Z_{\text{proxy}}^{\infty}\right\} \approx \text{Re}\left\{Z_{\text{dyn}}^{\infty}\right\} \tag{3}$$

where $Z_{\text{proxy}}^{\infty}$ is the dynamic component of the proxy dipole in the absence of the reflections. As the discretization of the proxy dipole is much coarser than the original one, it has a larger feeding gap, and consequently a negligible quasi-static component. The condition (3) for the synthesis is imposed only on the dynamic part the far-field radiation is independent of the quasi-static part Z_{qs}, which can be added in postprocessing. Using the separation of the wave phenomena as in Section II-B and using (3), the input impedance of the proxy dipole can be approximated as follows:

$$Z_{\text{proxy}} \approx \text{Re}\left\{Z_{\text{dyn}}^{\infty}\right\} + \text{Im}\left\{Z_{\text{proxy}}^{\infty}\right\} + Z_{\text{proxy}}^{\text{refl}}. \tag{4}$$

Since the original and the proxy dipoles have been synthesized in (3) to radiate equivalently, it is reasonable to assume that

$$Z_{\text{proxy}}^{\text{refl}} \approx Z^{\text{refl}}. \tag{5}$$

Therefore, the reflections can be extracted from (4) as follows:

$$Z^{\text{refl}} \approx Z_{\text{proxy}} - \text{Re}\left\{Z_{\text{dyn}}^{\infty}\right\} - \text{Im}\left\{Z_{\text{proxy}}^{\infty}\right\}. \tag{6}$$

Then, the input admittance of the original dipole in the finite medium can be estimated as follows:

$$Z_{\text{in,dyn}} \approx Z_{\text{dyn}}^{\infty} + Z_{\text{proxy}}^{\text{refl}}. \tag{7}$$

Finally, the input impedance can be obtained by adding Z_{qs} in parallel

$$Z_{\text{in}} = Z_{\text{in,dyn}} \| Z_{\text{qs}}. \tag{8}$$

Z_{dyn}^{∞} is calculated with the extraction of Z_{qs} from the input impedance of the original dipole radiating in the absence of the reflections. There are no constraints on the methods used to derive this latter, which can be evaluated with a commercial solver, a spectral domain representation [24], or with the same in-house full-wave solver used to extract the reflections. The final steps (7) and (8) can be represented by the equivalent circuit in Fig. 2(c).

IV. Results and Applications

A. Dielectric Lens Fed by a Single Dipole

The first example simulates with a volumetric method of moments (V-MoM) based on [26], [27], [28], [29], [30], [31] a dipole long $\ell = 0.5$ mm placed on the focus of an elliptical lens with a diameter 2 mm and dielectric permittivity $\varepsilon_r = 2.34$ [Fig. 4(a) and (b)]. The dipole has a square cross section with a side $w_y = w_z = 10$ μm, and it is fed by a δ-gap generator $\delta = 20$ μm long, as shown in Fig. 4(b). A structured mesh would require a discretization of at least 10 μm, i.e., the side of the cross section, yielding 16×10^6 unknowns. With the

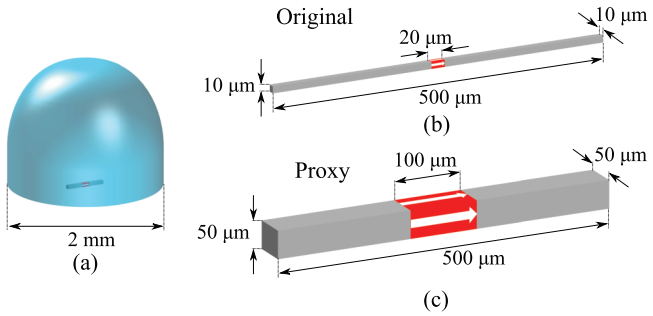

Fig. 4. Sketch of (a) lens fed by a dipole, (b) original dipole, and (c) proxy one.

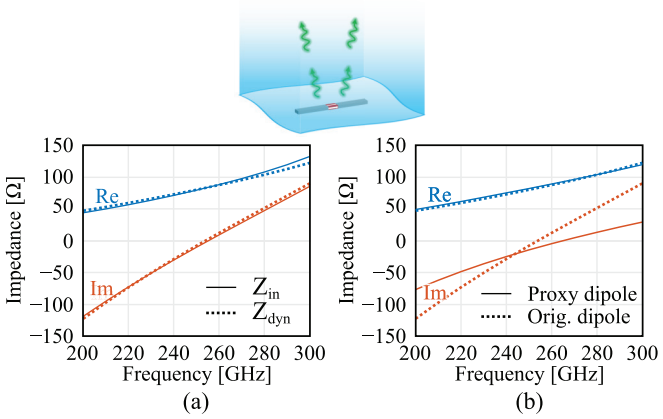

Fig. 5. (a) Input impedance and its dynamic component, of the original dipole radiating in the semi-infinite medium, and (b) synthesis of the proxy dipole.

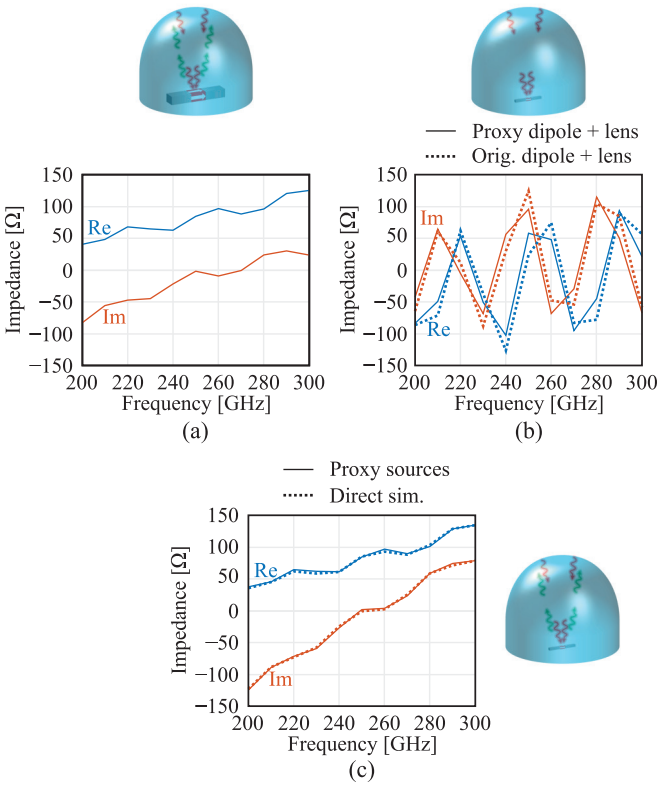

Fig. 6. (a) Input impedance of the proxy dipole illuminating the lens, (b) reflection component of the impedance extracted from the proxy and the original dipole, and (c) input impedance of the original dipole illuminating the lens simulated with the proxy sources method and with the direct simulation.

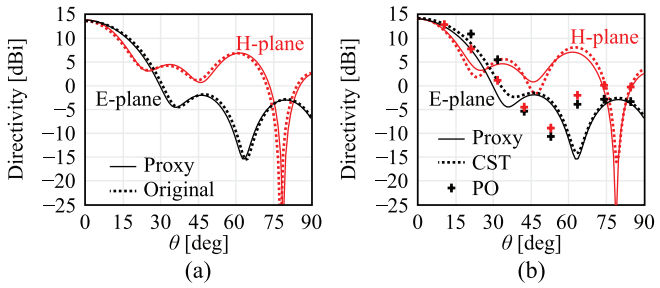

Fig. 7. Directivity plots of the lens (a) illuminated by the proxy and the original dipole and (b) assessed with the proxy sources method, CST, and the PO.

proposed method, it is possible to use the V-MoM and a structured mesh and achieve comparable results using a proxy dipole having a square cross section of 50 μm [Fig. 4(c)], and 141 $\times$ 10^3 unknowns for the entire problem.

The original dipole is first simulated with the method of moments when radiating at the interface between the free space and an dielectric half-space with permittivity $\varepsilon_r = 2.34$, and its impedance in the absence of reflections is calculated. The quasi-static impedance Z_{qs} is then isolated, and the dynamic component Z_{dyn} is shown in Fig. 5(a), where it is compared with the total input impedance. The proxy dipole is synthesized with the method of moments, by changing the cross section, the gap length, and the length of a much coarsely discretized dipole until minimizing the difference between the real parts of Z^{∞}_{proxy} and Z^{∞}_{dyn}. The input impedance of the proxy dipole is shown in Fig. 5(b). Then, the proxy dipole radiating into the lens is efficiently simulated, thanks to the coarse discretization, and its input impedance is shown in Fig. 6(a). The reflections Z^{refl} are then extracted with (6) and are shown in Fig. 6(b). Finally, the input impedance of the original dipole is estimated with (8), and its values are shown in Fig. 6(c), where these are compared with the direct simulation. Note that the direct full-wave simulation is possible to perform due to the relatively small size of the problem. In Fig. 6(b), the reflections from the lens extracted with the original dipole are compared with those extracted with the proxy one. This successful comparison proves that the specific geometry of the feed does not affect the interaction with the lens if it is equivalently radiating in the far-field.

In Fig. 7(a), the directivity patterns of the proxy and original problems are compared in the E- and H-planes. Due to the condition (3) and the fact that the details of the feed do not affect the far-field, the original and proxy dipoles share the same pattern. In Fig. 7(b), the directivity patterns of the lens fed by the proxy dipole are shown at 250 GHz, and the values obtained with the proposed method are compared with CST and the PO [21]. As the PO fields have been calculated for $\theta \in [0^\circ\ 90^\circ]$, the patterns of the method of moments and CST are normalized to the power radiated in the upper hemisphere only. The patterns obtained by the proposed method are in excellent agreement with CST, while the larger error committed by the PO further confirms its inaccuracy for the study of small lens antennas.

To show the validity of this procedure for off-focus dipoles, the feed of the previous geometry is shifted by 750 μm on the H-plane, an extreme configuration, considering that the lens radius is 1 mm. As the synthesis does not depend on the geometry of the surrounding dielectric, the synthesized proxy dipole is still the one of Figs. 4(c) and 5(b). The input impedance is compared in Fig. 8(a) with the standard simulation of the dipole displaced under the lens, showing an excellent agreement. The patterns on the H-plane at 250 GHz are shown in Fig. 8(b), where the directivity calculated

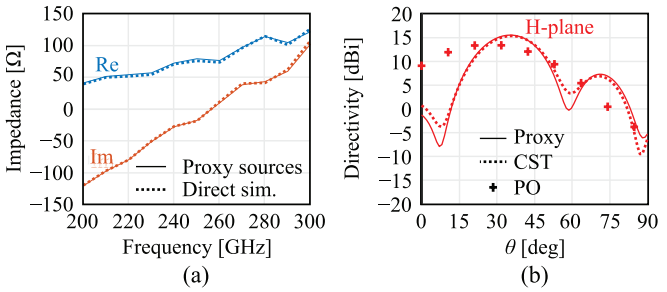

Fig. 8. (a) Comparison between the input impedance calculated for the shifted dipole with the proxy sources method and the direct simulation and (b) directivity in the H-plane calculated at 250 GHz with the method of moments (proxy sources), CST, and the PO.

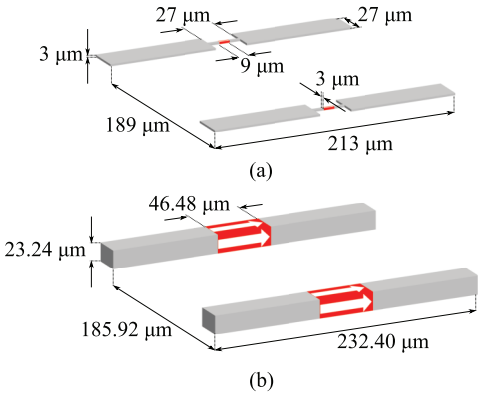

Fig. 9. Representation of (a) original dipole and (b) proxy double dipole.

with this method is compared with CST and PO. As before, the directivity is calculated by considering the power radiated in the upper hemisphere. While the patterns calculated with the proxy sources maintain a good accuracy also in off-focus configurations, the PO commits larger errors.

B. Dielectric Lens Fed by a Double-Dipole

The procedure can be extended to the analysis of a dielectric lens with relative permittivity $\varepsilon_r = 2.34$ fed by the double-dipole shown in Fig. 9(a). Due to the presence of the two feeding gaps, the synthesis of the proxy dipoles is carried out on the active impedances, i.e., the impedances when both the dipoles are excited. The original double-dipole radiating in the semi-infinite medium is obtained with a CST simulation, as the high level of detail implies a computational burden that is too heavy for the V-MoM with a structured mesh. Then, the quasi-static component is extracted from a single dipole as this is only due to the capacitive effects around the gap and does not impact on the mutual coupling between the dipoles. The two proxy dipoles in an array configuration are synthesized with the method of moments, resulting into the coarser and simpler geometry shown in Fig. 9(b). The synthesis results are shown in terms of active input impedance in Fig. 10(a). The double-dipole is used to illuminate from its focus a dielectric lens with a diameter of 1 mm. The input impedance calculated with the proxy sources method and the method of moments is compared with the direct CST simulation in Fig. 10(b), where it shows a good agreement. This example shows that the proxy sources method can be used for the analysis of complex realistic feeds. Moreover, this case of study also proves the flexibility of the method, as it shows that the simulation of a radiator close to a dielectric body can be simplified by separating the feed from the interaction with the body, where these two contributions can be simulated with different approaches. Finally, the patterns on the E- and H-planes at

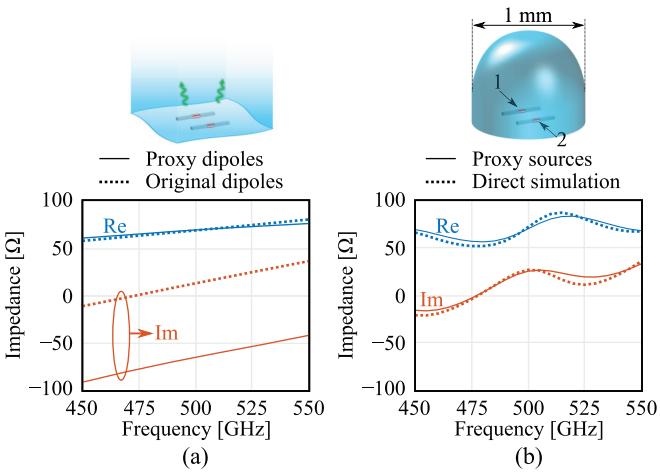

Fig. 10. (a) Synthesis of the proxy double dipole and (b) input impedance of the lens fed by the double-dipole calculated with the proxy sources method and with the direct simulation.

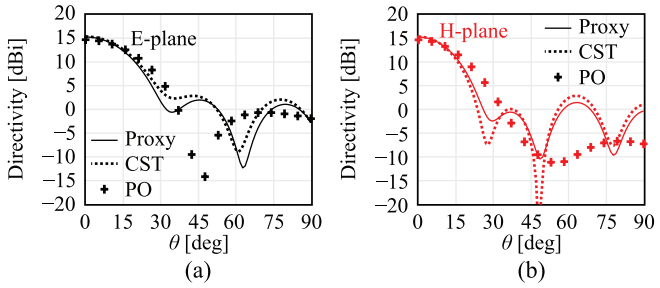

Fig. 11. Directivity patterns at 500 GHz in (a) E-plane and (b) H-plane.

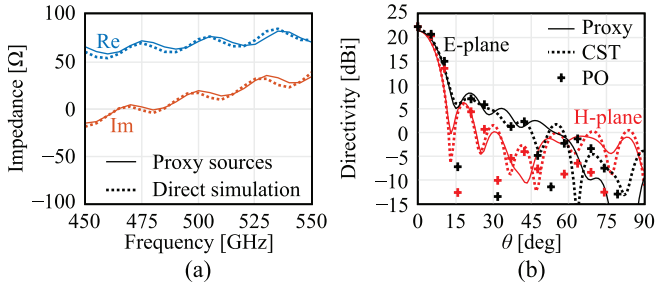

Fig. 12. (a) Comparison of the input impedance of the lens calculated with the proxy sources method and with the direct simulation and (b) directivity patterns in the E- and H-planes at 500 GHz.

500 GHz are shown in Fig. 11(a) and (b), respectively, showing a better agreement with CST rather than with the PO.

To test the potential of this method, the same feed of Figs. 9(a) and 10(a) is used to illuminate a larger lens with a diameter of 2.5 mm. The results in terms of the input impedance and the patterns are shown in Fig. 12 for the double-dipole placed in the focus.

C. Time Performance Analysis

The time performance analysis is summarized in Table I for the calculation of the input impedance of Figs. 6(c) and 10(b). The solution times of the proxy sources method presented in this communication, and carried out with the V-MoM code without the use of any preconditioner, are compared against the direct simulation, which depending on the case is performed with the V-MoM or CST. The use of the proxy sources method allows a reduction of the

TABLE I

SOLUTION TIME FOR THE INPUT IMPEDANCE CALCULATED AT INTEL[1] XEON[1] W-2265 CPU AT 3.5 GHZ, RAM 128 GB

	Proxy sources	Direct simulation	Time ratio
Fig. 6(c) (11 freq. points)	46 s	11 088 s (V-MoM)	0.4%
Fig. 10(b) (21 freq. points)	99 s	190 s (CST)	52%

TABLE II

SOLUTION TIME FOR THE DIRECTIVITY PATTERNS CALCULATED AT INTEL[1] XEON[1] W-2265 CPU AT 3.5 GHZ, RAM 128 GB

	Proxy sources	Original	PO‡	Time ratio
Fig. 7	21 s†	2288 s† (V-MoM) 46 s (CST)	26 s	0.9% (V-MoM) 46% (CST)
Fig. 11	32 s†	100 s (CST)	26 s	32%

† Computation time of the directivity patterns and average solution time from Table I.

‡ Computation time of the secondary patterns only.

solution times to 0.4% of the direct V-MoM simulation for Fig. 6(c) and to 52% of the CST simulation for Fig. 10(b).

In Table II the solution times for the calculation of the directivity patterns are reported. The proxy sources method performed with the V-MoM is compared against the direct simulation of the original problem, carried out with the V-MoM or CST, and the PO. The data reported for the proxy sources include the average solution time extracted from the corresponding entry in Table I and the time to calculate the directivity patterns from the currents. The use of the proxy sources reduces the calculation time of the directivity patterns to 0.9% of the direct V-MoM for Fig. 7. When compared with the direct CST simulation, for Figs. 7 and 11, the time ratio is 46% and the 32% with respect to the original simulations, respectively. Despite the calculation of the directivity having a computation time comparable with the one of the PO, it has to be noted that this latter does not account for the evaluation of the primary patterns.

It is worth mentioning that different scanning configurations do not alter the solution time.

V. CONCLUSION

The equivalent circuit representation of a feed illuminating a dielectric lens antenna is derived. This separates the capacitance of the feeding gap from the reflections created by the finite dielectric and from the propagation in an unbounded medium. This allows for the formulation of the proxy sources method to ease the full-wave simulations of integrated lens antennas. The input impedance can be calculated by combining the impedance in the absence of the reflections with the reflections extracted from the lens fed by the proxy feed. The impedance in the unbounded medium can be obtained with fast full-wave simulations or a semi-analytical solution such as [24]. The proxy dipole has the same interaction with the lens, but it is coarser than the actual one, therefore allowing efficient full-wave simulations.

The method is validated against the PO and against direct simulations obtained with either commercial solvers or in-house codes. While it shows up-to-par accuracy with respect to full-wave solvers, it proves better performance than the PO, especially when dealing with small-size lenses.

[1]Registered trademark.

ACKNOWLEDGMENT

The authors wish to thank Dr. Shahab O. Dabironezare for his help with the physical optics results.

REFERENCES

[1] D. F. Filipovic, S. S. Gearhart, and G. M. Rebeiz, "Double-slot antennas on extended hemispherical and elliptical silicon dielectric lenses," *IEEE Trans. Microw. Theory Techn.*, vol. 41, no. 10, pp. 1738–1749, Oct. 1993.

[2] J. M. Edwards, R. O'Brient, A. T. Lee, and G. M. Rebeiz, "Dual-polarized sinuous antennas on extended hemispherical silicon lenses," *IEEE Trans. Antennas Propag.*, vol. 60, no. 9, pp. 4082–4091, Sep. 2012.

[3] A. J. Alazemi, H.-H. Yang, and G. M. Rebeiz, "Double bow-tie slot antennas for wideband millimeter-wave and terahertz applications," *IEEE Trans. THz Sci. Technol.*, vol. 6, no. 5, pp. 682–689, Sep. 2016.

[4] K. Konstantinidis et al., "Low-THz dielectric lens antenna with integrated waveguide feed," *IEEE Trans. THz Sci. Technol.*, vol. 7, no. 5, pp. 572–581, Sep. 2017.

[5] M. A. Campo, D. Blanco, S. Bruni, A. Neto, and N. Llombart, "On the use of Fly's eye lenses with leaky-wave feeds for wideband communications," *IEEE Trans. Antennas Propag.*, vol. 68, no. 4, pp. 2480–2493, Apr. 2020.

[6] M. A. Campo et al., "H-band quartz-silicon leaky-wave lens with air-bridge interconnect to GaAs front-end," *IEEE Trans. THz Sci. Technol.*, vol. 11, no. 3, pp. 297–309, May 2021.

[7] M. Hoogelander et al., "Chessboard focal plane array for a CMOS-integrated terahertz camera," *IEEE Trans. THz Sci. Technol.*, vol. 13, no. 6, pp. 704–717, Nov. 2023.

[8] J. L. González-Jiménez et al., "A D-band transmitter achieving 57.6-Gb/s and 30-dBm EIRP based on channel-aggregation 45-nm ICs and a low-profile flat lens antenna," *IEEE Trans. Microw. Theory Techn.*, vol. 72, no. 1, pp. 836–850, Jan. 2024.

[9] H. Zhang, S. Bosma, A. Neto, and N. Llombart, "A dual-polarized 27 dBi scanning lens phased array antenna for 5G point-to-point communications," *IEEE Trans. Antennas Propag.*, vol. 69, no. 9, pp. 5640–5652, Sep. 2021.

[10] N. V. Rooijen et al., "A core-shell lens for antenna on-package integration at D-band," *IEEE Trans. Antennas Propag.*, vol. 72, no. 8, pp. 6195–6208, Aug. 2024.

[11] E. Lima, J. R. Costa, M. G. Silveirinha, and C. A. Fernandes, "ILASH–software tool for the design of integrated lens antennas," in *Proc. IEEE Antennas Propag. Soc. Int. Symp.*, San Diego, CA, USA, Jul. 2008, pp. 1–4.

[12] J. Budhu and Y. Rahmat-Samii, "A novel and systematic approach to inhomogeneous dielectric lens design based on curved ray geometrical optics and particle swarm optimization," *IEEE Trans. Antennas Propag.*, vol. 67, no. 6, pp. 3657–3669, Jun. 2019.

[13] A. Paraskevopoulos, F. Maggiorelli, M. Albani, and S. Maci, "Radial GRIN lenses based on the solution of a regularized ray congruence equation," *IEEE Trans. Antennas Propag.*, vol. 70, no. 2, pp. 888–899, Feb. 2022.

[14] Q. Liao, N. J. G. Fonseca, M. Camacho, Á. Palomares-Caballero, F. Mesa, and O. Quevedo-Teruel, "Ray-tracing model for generalized geodesic-lens multiple-beam antennas," *IEEE Trans. Antennas Propag.*, vol. 71, no. 3, pp. 2640–2651, Mar. 2023.

[15] P. Castillo-Tapia, J. Rico-Fernández, S. Clendinning, F. Mesa, and O. Quevedo-Teruel, "Evaluation of losses in 3-D-Printed geodesic lenses using a ray-tracing model," *IEEE Trans. Antennas Propag.*, vol. 72, no. 1, pp. 234–242, Jan. 2024.

[16] M. Chen, O. Habiboglu, F. Mesa, and O. Quevedo-Teruel, "Ray-tracing and physical-optics model for planar Mikaelian lens antennas," *IEEE Trans. Antennas Propag.*, vol. 72, no. 2, pp. 1735–1744, Feb. 2024.

[17] W. Hu, C. M. C. Martin, and D. Cavallo, "Design formulas for flat gradient index lenses with planar or spherical output wavefront," *IEEE Trans. Antennas Propag.*, vol. 72, no. 3, pp. 2555–2563, Mar. 2024.

[18] I. Gashi, A. Paraskevopoulos, S. Maci, and M. Albani, "GO analysis of GRIN lens antennas by combining in a single ODE, field and wavefront-curvature transport to the ray tracing," *IEEE Trans. Antennas Propag.*, vol. 72, no. 3, pp. 2147–2160, Mar. 2024.

[19] M. Pubill-Font, F. Mesa, A. Algaba-Brazález, S. Clendinning, M. Johansson, and O. Quevedo-Teruel, "2-D ray-tracing model for multilayer dielectric dome arrays with inner reflections," *IEEE Open J. Antennas Propag.*, vol. 5, pp. 845–854, 2024.

[20] S. Oddin Dabironezare, A. Nair, A. Neto, and N. Llombart, "Estimation of mutual coupling in integrated lens arrays using a geometrical optics-based technique with bi-directional forward ray-tracing," *IEEE Trans. Antennas Propag.*, vol. 72, no. 6, pp. 4796–4805, Jun. 2024.

[21] H. Zhang, S. O. Dabironezare, G. Carluccio, A. Neto, and N. Llombart, "A Fourier optics tool to derive the plane wave spectrum of quasi-optical systems [EM programmer's notebook]," *IEEE Antennas Propag. Mag.*, vol. 63, no. 1, pp. 103–116, Feb. 2021.

[22] G. Godi, R. Sauleau, and D. Thouroude, "Performance of reduced size substrate lens antennas for millimeter-wave communications," *IEEE Trans. Antennas Propag.*, vol. 53, no. 4, pp. 1278–1286, Apr. 2005.

[23] E. A. Speksnijder, R. Ozzola, and A. Neto, "Spectral domain Green's function of an infinite dipole with non-zero metal thickness and rectangular cross-section," *IEEE Trans. Microw. Theory Techn.*, vol. 72, no. 8, pp. 4530–4541, Aug. 2024.

[24] R. Ozzola, C. Tadolini, and A. Neto, "Spectral domain analysis of lossy and nonzero thickness dipoles of finite length radiating in layered media," *IEEE Trans. Antennas Propag.*, vol. 72, no. 11, pp. 8888–8892, Nov. 2024.

[25] A. Neto, S. Maci, and P. J. I. de Maagt, "Reflections inside an elliptical dielectric lens antenna," *IEE Proc. Microw., Antennas Propag.*, vol. 145, no. 3, p. 243, 1998.

[26] J. Markkanen, P. Yla-Oijala, and A. Sihvola, "Discretization of volume integral equation formulations for extremely anisotropic materials," *IEEE Trans. Antennas Propag.*, vol. 60, no. 11, pp. 5195–5202, Nov. 2012.

[27] A. D. Polimeridis, J. F. Villena, L. Daniel, and J. K. White, "Stable FFT-JVIE solvers for fast analysis of highly inhomogeneous dielectric objects," *J. Comput. Phys.*, vol. 269, pp. 280–296, Mar. 2014.

[28] M. C. van Beurden and S. J. L. van Eijndhoven, "Well-posedness of domain integral equations for a dielectric object in homogeneous background," *J. Eng. Math.*, vol. 62, no. 3, pp. 289–302, Nov. 2008.

[29] A. A. Tambova, M. S. Litsarev, G. Guryev, and A. G. Polimeridis, "On the generalization of DIRECTFN for singular integrals over quadrilateral patches," *IEEE Trans. Antennas Propag.*, vol. 66, no. 1, pp. 304–314, Jan. 2018.

[30] M. F. Catedra, E. Gago, and L. Nuno, "A numerical scheme to obtain the RCS of three-dimensional bodies of resonant size using the conjugate gradient method and the fast Fourier transform," *IEEE Trans. Antennas Propag.*, vol. 37, no. 5, pp. 528–537, May 1989.

[31] R. Ozzola, C. Tadolini, E. A. Speksnijder, and A. Neto, "Full-wave lens antenna analysis with the proxy sources method: Additional material," *IEEE Trans. Antennas Propag.*, to be published.